



Research Article

Fermat polynomial-based machine learning algorithm for a few non-linear ship roll damping models arising in ship dynamics

S. Krithikka^a, G. Hariharan^{a,*}, H. Jafari^{b,c,d,e,*}

^aDepartment of Mathematics, SASTRA Deemed University, School of Arts, Sciences, Humanities and Education, SASTRA, Thanjavur, 613401, India

^bDepartment of Mathematics, Saveetha School of Engineering, Saveetha Institute of Medical and Technical Sciences (SIMATS), Chennai 602105, TamilNadu, India

^cDepartment of Applied Mathematics, University of Mazandaran, Babolsar, Iran

^dDepartment of Mathematical Sciences, University of South Africa, UNISA0003, Pretoria, South Africa

^eDepartment of Medical Research, China Medical University Hospital, China Medical University, Taichung 110122, Taiwan

ARTICLE INFO

Keywords:

Barge-like vessel model
Fermat's polynomials
Homotopy perturbation method
Machine learning
Non-linear differential equations

ABSTRACT

Roll damping significantly influences ship dynamical models, playing a key role in predicting vessel behavior. Recently, in [Ocean Engineering 264 (2022) 112390] discussed the study, which considers a floating production storage and offloading (FPSO) tank model and a barge-like vessel model that consists of two spherical tanks, each governed by different restoring moments and damping coefficients to capture their unique dynamic behaviors. The Lucas wavelet method, along with the multi-layer perceptron approach, has been used for parameter estimations to the observed model. In this study, a machine-learning-based model—multi layer perceptron (MLP)—is employed to predict the roll angle of the ship by incorporating both the restoring moments and damping coefficients results obtained using the fermat polynomial method (FPM). The non-linear differential equations are transformed into simple algebraic equations by considering appropriate collocation points by utilizing derivatives of operational matrices. Accuracy and effectiveness of the proposed FPM-based approximation are validated using experimental data from frozen cargo conditions and validated with the homotopy perturbation method (HPM) results. The obtained solution is compared with a few numerical methods and experimental results. However, the FPM solutions are easy to investigate, straightforward, and convenient algorithms for solving differential equations that are non-linear and arise in ship dynamics.

1. Introduction

The movement of a ship is influenced by waves, associated with six degrees of freedom of the ship dynamical models. Out of six, roll motion, in particular, is of major concern because it has the potential to capsize the vessel. Most roll models share common structures, differing mainly in how they represent damping, restoring forces, and added mass. Estimation of parameters is essential for accurately predicting roll behavior, especially under resonance conditions in real-time applications. The complex nature of restoring and damping forces adds to the model of the motion, as many non-linear roll damping models exhibit strong nonlinearity. Because exact solutions for non-linear roll models exist but are hard to find analytically, approximation techniques have been developed to address these models in both the time and frequency domains.

Recent studies have concentrated on estimating parameters for ship roll behavior through a range of approaches, such as analytical investigations, scale-model testing, and numerical simulations. These techniques are designed to evaluate the vessel's roll response, including angular displacement, oscillation magnitude, energy dissipation, and restoring forces. The roll response is often tackled using non-linear differential equations, and many studies have applied semi-analytical or numerical methods to provide approximate solutions in situations

where exact answers are not available. These approximations do not always fully capture the qualitative behavior of the solutions.

One promising approach to the ship dynamics in parameter estimation is the use of wavelet methods, which are effective in analyzing free decay signals. Wavelets, generated through shifts and scaling of a mother function, provide significant benefits in signal processing, including localized support, multi-resolution capability, and orthonormal properties. These features make wavelets useful for converting problems into simpler forms, which are then solved by various numerical methods. The capacity of wavelets to achieve localization in both time and frequency domains, along with their adaptability, has made them a powerful tool in solving any differential equations that arise in science and engineering.

Wavelets have found applications in diverse fields, such as applied mathematics, physics, engineering, and statistics, particularly in time series analysis. Wavelet neural networks (WNN) have emerged as a strong computational algorithm for solving non-linear and fractional differential equations, although selecting the right mother wavelet function remains a challenge. This study presents a machine learning-assisted computational approach for directly solving non-linear ship roll equations, eliminating the need for transformation formulas or limiting assumptions. The fermat polynomial method (FPM) is validated against established analytical solutions and experimental data, demonstrating

*Corresponding authors:

E-mail addresses: jafarh@unisa.ac.za (H. Jafari), hariharan@maths.sastra.edu (G. Hariharan)

Received: 29 May, 2025 Accepted: 29 December, 2025 Epub Ahead of Print: 06 April, 2026 Published: 16 April, 2026

DOI: 10.25259/JKSUS_952_2025

its effectiveness as a robust tool for simulating and forecasting ship roll dynamics. By integrating multi-layer perceptron (MLP) models, the method provides the real-time predictions, particularly in forecasting sudden increases in wave height in ship dynamics.

Hosseini et al. (2021), presented a spectral collocation scheme to compute numerical solutions of stochastic multi-term time-fractional diffusion problems with Brownian-driven noisy input, modelling symmetry breaking in molecular oscillations. Using sixth-kind Chebyshev polynomial-based collocation, the formulation is transformed into linear algebraic systems, with test cases confirming efficiency and precision. Jafari et al. (2024) described how multi-term time-fractional models extend classical convection–diffusion equations using Caputo derivatives, offering flexible representation of complex system dynamics. A fully meshless MLS-based scheme with weighted finite differences ensures accurate approximation across varied domains, demonstrating reliability and sensitivity to collocation choices. The study by Shadabfar et al. (2023) develops a fractional SEIR-VQHP model with Monte Carlo back analysis to estimate COVID-19 spread in the US, accounting for vaccination, quarantine, hospitalization, and social distancing. Results predict infection, recovery, and mortality trends, with sensitivity analysis showing that higher vaccination and stricter distancing significantly reduce cases.

The paper is presented as follows. Section 2 provides the mathematical dynamics of an floating production storage and offloading (FPSO) and a barge-like vessel equipped with two spherical tanks. In Section 3, the mathematical formulation of the proposed model is presented. In Section 4, the foundational concepts of Fermat polynomials and the operational matrix of derivatives are introduced. Section 5 details the numerical experiments conducted. Section 6 provides details of the results and their implications. The paper is concluded with key findings and closing remarks in Section 7. Future work is mentioned in Section 8.

2. Unveiling Model Dynamics

This section highlights the modelling of two offshore structures with distinct characteristics: the barge-like vessel, known for its simple hull geometry and pronounced roll response, and the FPSO, a complex floating unit designed for production and storage in harsh environments. Their dynamic behavior is explored to illustrate differences in hydrodynamic response, station-keeping, and operational challenges.

2.1 Barge-like vessel

To investigate the sloshing phenomenon and roll response, the measurement of a barge-like vessel is given as 200 meters in length and a beam of 46 meters—reflecting full-scale dimensions—was developed, as summarized in Table 1. The roll behavior of a Moss-type Liquefied Natural Gas (LNG) carrier is emulated by designing the vessel features with a uniform cross-sectional profile along its length. To simulate the sloshing effects, two spherical tanks were integrated. Consider the Deepwater Wave Basin at a 1:60 scale to perform the model testing. LNG carriers experience varying intermediate load conditions during side-by-side offloading operations; for this study, a 50% volume condition was selected as the reference case. Table 1 provides the corresponding specifications for both model-scale and full-scale vessels, and Fig. 1 shows the experimental model.

Table 1.
Barge-like vessel Mass Properties (Zhao and McPhail, 2017).

Designation	Full scale	Model scale
Perpendiculars Length (meter)	200	3.333
Width(meter)	46	0.767
Intensity(meter)	25.5	0.425
Average Draught(meter)	11.1	0.185
Vessel Displacement (kilogram)	99297900	459.7
Radius of roll gyration(meter)	19.4	0.323
Radius of pitch gyration(meter)	68.5	1.142



Fig. 1. Experimental Scale model (Zhao and McPhail, 2017)

Model tests were performed under both wave conditions and calm water. To obtain roll decay curves, the decay test in calm water is performed. During these tests, the considered model was initially heeled to a predetermined angle and, upon reaching the target inclination, was rapidly released to oscillate freely under still-water conditions.

2.2 Floating production storage and offloading (FPSO) model

The FPSO unit, representative of those commonly used on Brazilian oil platforms, was selected as a case study. To perform the model tests, a scale of 1:70 is taken, considering three distinct operational loading conditions: full load, intermediate load, and ballast. Table 2 summarizes the principal characteristics of the FPSO, while in Fig. 2, for each loading condition, the 3D perspective views of the hull are presented. The FPSO was outfitted with bilge keels in all scenarios measuring 1.00 meter in width, extending 127.2 meters along the parallel midbody on both the starboard and port sides. Notably, to enhance roll damping, FPSOs are typically fitted with larger bilge keels than conventional ships.

As shown in Fig. 2, roll decay tests were conducted for the FPSO under all three loading conditions. For each case, the test began with the largest initial roll angle specific to that loading scenario. The measured natural periods were 14.8 s, 14.4 s, and 14.2 s for the fully loaded, partial load condition, and ballast load conditions, respectively. Table 3 presents the estimated roll damping coefficients derived from the experimental model data.

3. Mathematical Representation

To systematically capture the motion and response of floating structures, their dynamics are expressed through mathematical formulations. This section outlines the governing equations of motion, incorporating hydrodynamic forces, restoring effects, and external excitations, thereby providing the foundation for analytical and numerical analysis.

Table 2.
FPSO model- mass properties (Rodríguez et al., 2020).

Designation	Fully loaded	Partial load condition	Ballast load
Perpendiculars length (meter)	320	320	320
Width(meter)	54.5	54.5	54.5
Intensity(meter)	27.8	27.8	27.8
Draught(meter)	21	14.7	8
Vessel Displacement (kilogram)	311.046	211.884	111.4
Roll Inertia(t.m.m)	1.09E+08	8.29E+07	5.09E+07
Metacentric height(meter)	7.9	9.5	12.41

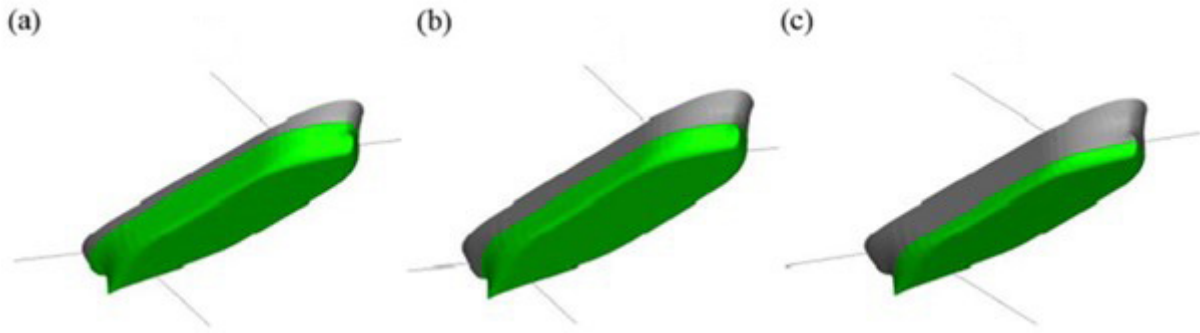


Fig. 2. Loading conditions of FPSO Model (a) fully loaded, (b) Partial load condition, (c) Ballast load (G. Swaminathan et al, 2022).

Table 3.
Coefficients of decay damping (Rodríguez et al., 2020).

Condition	Fully loaded		Partial load condition		Ballast load	
	B ₁ [1/s]	B ₂ [1/s]	B ₁ [1/s]	B ₂ [1/s]	B ₁ [1/s]	B ₂ [1/s]
Init 5°	0.02	0.192	NA	NA	NA	NA
Init 10°	0.015	0.555	0.015	0.71	0.029	1.056
Init 15°	0.014	0.586	NA	NA	NA	NA
Init 20°	NA	NA	0.018	0.705	0.057	0.415

3.1 A barge-like vessel configuration

The governing equation of the ship model, considering non-linear roll damping, is given by (Zhao et al., 2016a, 2016b):

$$(M + A)\ddot{\varphi} + B_1\dot{\varphi} + B_2\dot{\varphi}|\dot{\varphi}| + C\varphi = 0 \quad (1)$$

The decay oscillation is approximately harmonic in each half cycle. Based on this assumption, the linear and non-linear damping coefficients are computed. Therefore, Fourier series is used to linearize the non-linear term.

$$\dot{\varphi}|\dot{\varphi}| = \frac{8}{3\pi}\alpha_n\varphi_i\dot{\varphi} \quad (2)$$

In Eq. (1), by substituting Eq. (2), the non- dimensional form

$$\ddot{\varphi} + 2\gamma\alpha_n\dot{\varphi} + \epsilon\frac{8}{3\pi}\alpha_n\varphi_i\dot{\varphi} + \alpha_n^2\varphi = 0$$

Where γ represents the damping coefficient, α_n the natural frequency, and ϵ is a factor accounting for the non-linear term with an initial role angle 4^0 .

3.2 Model of FPSO

For FPSO, the equation of ship model in calm water can be denoted as (Zhao et al., 2016a):

$$(I_{44} + a_{44})\ddot{\varphi} + b_{44}(\varphi)\dot{\varphi} + C\varphi = 0, \quad (3)$$

where the damping coefficient is denoted by $b_{44}(\varphi)$. The Eq. (3) represents the canonical form and written as:

$$\ddot{\varphi} + b(\varphi)\dot{\varphi} + \alpha_n^2\varphi = 0,$$

where, Eq. (4)

$$b(\varphi) = \frac{b_{44}(\varphi)}{I_{44} + a_{44}} \text{ and } \alpha_n^2 = \frac{mgGM}{I_{44} + a_{44}} \quad (4)$$

The damping moment can be decomposed into linear and quadratic components:

$$b(\varphi)\dot{\varphi} = b_1\dot{\varphi} + b_2\dot{\varphi}|\dot{\varphi}|, \quad (5)$$

Put Eq. (5) into Eq. (4), the ship's roll motion equation:

$$\ddot{\varphi} + b_1\dot{\varphi} + b_2\dot{\varphi}|\dot{\varphi}| + \alpha_n^2\varphi = 0$$

with an initial roll angle of 10^0 .

4. Preliminaries - Fermat Polynomials

This section introduces the essential properties and operational rules of Fermat polynomials, which provide efficient basis functions for approximation. In parallel, the role of Multi-Layer perceptron (MLPs) is highlighted, illustrating how traditional polynomial-based methods can be combined with ML models to enhance flexibility, accuracy, and adaptability in solving complex differential equations.

With the use of a recurrence relation, the Fermat polynomial can be generated as:

$$F_{i+2}(y) = 3yF_{i+1}(y) - 2F_i(y) ; F_0(y) = 0, F_1(y) = 1, i \geq 0$$

These polynomials are specific instances of the (p,q)-Fibonacci polynomials, introduced in reference [11]. The general form of these polynomials is generated by the relation:

$$U_{i+2}(y) = p(y)U_{i+1}(y) - q(y)U_i(y) , i \geq 0$$

with initial conditions:

$$U_0(y) = 0, U_1(y) = 1$$

The Binet formula for $U_i(y)$ is given by:

$$U_i(y) = \frac{\alpha^i(y) - \beta^i(y)}{\alpha(y) - \beta(y)}, \quad i \geq 0$$

where:

$$\alpha(y) = \frac{p(y) + \sqrt{p(y)^2 + 4q(y)}}{2}, \quad \beta(y) = \frac{p(y) - \sqrt{p(y)^2 + 4q(y)}}{2}$$

For Fermat polynomials, we use $p(y)=3y$ and $q(y)=-2$.

In this work, Fermat polynomials are defined on the domain $y \in [0,1]$ with their explicit form given by:

$$F_k(y) = \frac{\left(3y + \sqrt{9y^2 - 8}\right)^k - \left(3y - \sqrt{9y^2 - 8}\right)^k}{2^k \sqrt{9y^2 - 8}}$$

The polynomials $F_{i+1}(y)$ have the following analytic form:

$$F_{i+1}(y) = \sum_{k=0}^{\lfloor i/2 \rfloor} (-2)^k 3^{i-2k} \binom{i-k}{k} y^{i-2k}.$$

Operational matrices of derivatives for Fermat polynomial method are given as follows:

$$D = \begin{bmatrix} 0 & 0 & 0 \\ 3 & 0 & 0 \\ 0 & 6 & 0 \end{bmatrix}; \quad D^2 = \begin{bmatrix} 0 & 0 & 0 \\ 0 & 0 & 0 \\ 0 & 36 & 0 \end{bmatrix}$$

Then the Fermat polynomial matrix is,

$$\psi(y) = \begin{bmatrix} 1 \\ 3y \\ 9y^2 - 2 \end{bmatrix}$$

4.1 FPM with MLP for time-forecasting

To expand the Fermat polynomial domain for forecasting purposes, a widely used feed-forward neural network, the MLP, is utilized. The roll angle data, which is inherently time-dependent, forms a time-series structure that is critical for accurate predictions. The MLP model's output was designed to rely on the past 1 s of roll angle history, ensuring improved forecast accuracy.

Fig. 3 illustrates the methodology for predicting future roll angle data using the MLP network's architecture (Swaminathan et al., 2022). After extracting the roll angle information using the wavelet-based method, it is passed to the initial stage of the multi-layer perceptron.

The architecture includes five internal processing layers followed by a final prediction layer, with each stage employing a sigmoid function to transform its signals. To optimize the learning process, the Adam optimizer—renowned for its efficiency in handling time-series data—was employed with an initial learning rate of 0.001.

With this network configuration, the MLP successfully predicted roll angle data for the next 200 s with remarkable accuracy, demonstrating the effectiveness of the proposed method for time-series forecasting.

5. Numerical Simulation and Experiments

To validate the proposed methodology, both numerical simulations and experimental investigations are carried out. The simulations provide controlled insights into system dynamics under varying conditions, while the experimental results offer practical evidence of accuracy and applicability. Together, they form a comprehensive evaluation framework, bridging theoretical development with real-world performance.

5.1 Non-linear ship roll motion model for goods type ships

The derived non-linear roll motion ship Eq. (1) along with its associated initial conditions is written as (Swaminathan et al. (2022))

$$\frac{d^2\varphi}{dt^2} + b_1 \frac{d\varphi}{dt} + b_2 \frac{d\varphi}{dt} \left| \frac{d\varphi}{dt} \right| + C_1 \varphi = 0, \tag{6}$$

Under the initial conditions

$$\varphi(0) = 0.0698132, \quad \varphi'(0) = 0.$$

Here b_1 and b_2 are damping moments and C_1 is restoring moment.

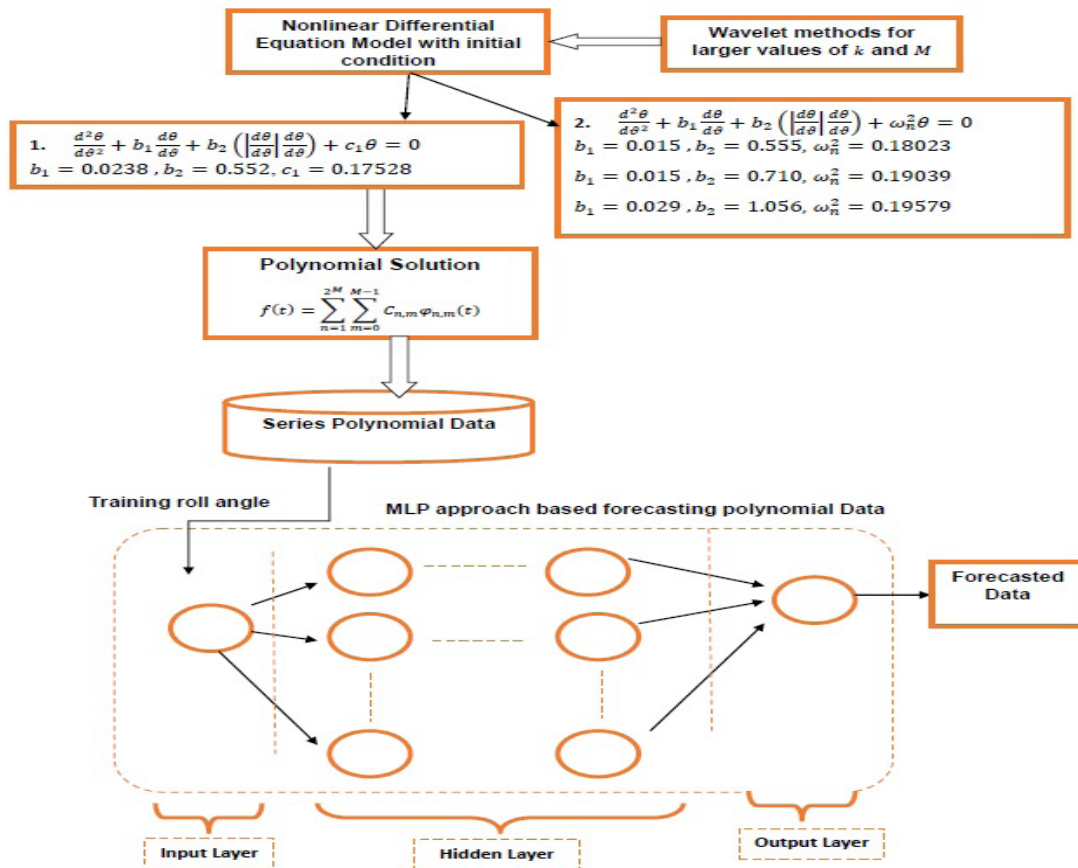


Fig. 3. Multi-layer perceptron based on FPM results flowchart.

Then the FPM is given using $b_1=0.0238$, $b_2=0.552$, $C_1=0.17528$ and the collocation point as $x=0.47$, Eq. (6) becomes,

$$4.968C_1^2 + C_1(28.0195C_2 + 0.0714) + 39.5075C_2^2 + 50.9613C_2 + 0.0823 = 0. \tag{7}$$

Under the given initial conditions, we have the following equations

$$\varphi(0) = 0.0698132 \Rightarrow C_0 = 0.0698132 + 2C_2; \varphi^I(0) = 0 \Rightarrow C_1 = 0. \tag{8}$$

Therefore, by solving Eq. (7) and Eq. (8), we get the connection coefficients

$$C_0 = 0.0658, C_1 = 0, C_2 = -0.002.$$

Hence, we get the Fermat polynomial solution as

$$\varphi(t) = 0.0698132 - 0.018t^2.$$

homotopy perturbation method (HPM) solution:

$$\begin{aligned} \varphi(t) &= -0.018t^2 + 0.004888t + 0.0698 \\ &+ \left(0.001709 \int_0^\infty t \cos(0.4187t) |t| dt - 0.002 \right) \sin(0.4187t) \\ &- 0.001709 \cos(0.4187t) \int_0^\infty t \sin(0.4187t) |t| dt. \end{aligned}$$

5.2 Non-linear ship roll motion model with linear and quadratic restoring and damping coefficients

The derived non-linear roll motion ship Eq. (1), along with its associated initial conditions, is written as (Swaminathan et al., 2022)

$$\frac{d^2\varphi}{dt^2} + b_1 \frac{d\varphi}{dt} + b_2 \frac{d\varphi}{dt} \left| \frac{d\varphi}{dt} \right| + \alpha_n^2 \varphi = 0, \tag{9}$$

Under the initial conditions

$$\varphi(0) = 0.174533 \text{ and } \varphi'(0) = 0$$

Here, b_1 and b_2 are damping moments and α_n^2 is the quadratic restoring moment. The various parameter values are chosen in each case below because they are experimentally measured for damping and natural period of FPSO roll motion under different load conditions.

Case 1:

Using $b_1=0.015$, $b_2=0.555$, $\alpha_n^2=0.18023$ and the collocation point as $x=0.47$, Eq.(9) becomes

$$4.995C_1^2 + C_1(28.1718C_2 + 0.045) + 39.7222C_2^2 + 50.8869C_2 + 0.0847 = 0. \tag{10}$$

Under the given initial conditions, we have the following equations,

$$\varphi(0) = 0.174533 \Rightarrow C_0 = 0.174533 + 2C_2; \varphi^I(0) = 0 \Rightarrow C_1 = 0. \tag{11}$$

Using Eq. (10) and Eq. (11), we get the connection coefficients

$$C_0 = 0.170533, C_1 = 0, C_2 = -0.002.$$

The FPM solution is obtained by using the connection coefficients,

$$\varphi(t) = 0.174533 - 0.018t^2.$$

Using $\varepsilon = 0.01$, the HPM solution is

$$\begin{aligned} \varphi(t) &= 0.174533 \cos(0.42440t) + \varepsilon(0.174533 \sin(0.42440t) \\ &- 0.2295 \cos(0.42440t)). \end{aligned}$$

Case 2:

Consider $b_1=0.015$, $b_2=0.710$, $\alpha_n^2=0.19039$ and the collocation point as $x=0.47$. Then, Eq. (9) becomes

$$6.39C_1^2 + C_1(36.0396C_2 + 0.045) + 50.8158C_2^2 + 50.8869C_2 + 0.08948 = 0. \tag{12}$$

With the help of the initial conditions, we have the following equations

$$\varphi(0) = 0.174533 \Rightarrow C_0 = 0.174533 + 2C_2; \varphi^I(0) = 0 \Rightarrow C_1 = 0. \tag{13}$$

Solving Eq. (12) and Eq. (13), we get the connection coefficients

$$C_0 = 0.170533, C_1 = 0 \text{ and } C_2 = -0.002.$$

With the help of the above connection coefficients, we gain

$$\varphi(t) = 0.174533 - 0.018t^2.$$

Using $\varepsilon = 0.01$, the HPM solution is as follows:

$$\begin{aligned} \varphi(t) &= 0.174533 \cos(0.436t) + \varepsilon(0.170533 \sin(0.436t) \\ &- 0.555 \cos(0.436t)). \end{aligned}$$

Case 3:

By applying $b_1=0.029$, $b_2=1.056$, $\alpha_n^2=0.19579$ and the collocation point as $x=0.47$, then Eq. (9) becomes

$$9.504C_1^2 + C_1(53.6026C_2 + 0.087) + 75.5796C_2^2 + 51.0053C_2 + 0.09202 = 0.$$

By applying the given initial conditions, we have the following equations

$$\varphi(0) = 0.174533 \Rightarrow C_0 = 0.174533 + 2C_2; \varphi^I(0) = 0 \Rightarrow C_1 = 0.$$

Solving the above equations, we get the connection coefficients

$$C_0 = 0.170533, C_1 = 0, C_2 = -0.002.$$

FPM Solution:

$$\varphi(t) = 0.174533 - 0.018t^2.$$

Using $\varepsilon = 0.01$, HPM solution is as follows:

$$\begin{aligned} \varphi(t) &= 0.174533 \cos(0.442t) + \varepsilon(0.174533 \sin(0.442t) \\ &- 0.4245 \cos(0.442t)). \end{aligned}$$

6. Results and Discussion

This section presents the obtained results and provides a detailed discussion of their significance. Numerical findings are compared with experimental data to assess accuracy, while key trends and deviations are analyzed to highlight the strengths and limitations of the proposed approach. The discussion further interprets the physical meaning of the results and their implications for practical applications.

In Table 4, the roll angle responses are compared across three different sources: the Frozen Cargo results from Zhao et al. (2016a), the semi-analytical HPM, and the proposed FPM. The Frozen Cargo data serves as the benchmark because it is derived from experimental and numerical studies on a barge-like vessel with spherical cargo tanks and thus reflects realistic roll decay behavior. HPM and FPM are included as established solution techniques for non-linear roll equations, providing analytical approximation and direct numerical integration, respectively. The inclusion of these data sources ensures that the proposed FPM is validated against the experimental benchmark and widely accepted

Table 4. Numerical result Comparison of roll angle with experimental data (Frozen cargo) (Zhao et al., 2016a) and (Wenhua Zhao et al, 2016), HPM and FPM

t(Sec.)	Frozen Cargo	HPM	FPM
0	4	4	4
0.053	3.937	4.0086	3.997
0.105	3.876	4.0122	3.989
0.158	3.818	4.0102	3.974
0.211	3.763	4.0023	3.954
0.263	3.71	3.989	3.929
0.316	3.659	3.9697	3.897
0.368	3.61	3.9451	3.86
0.421	3.563	3.9144	3.817
0.474	3.518	3.8779	3.768
0.526	3.475	3.8364	3.715
0.579	3.433	3.7885	3.654
0.632	3.393	3.7349	3.588
0.684	3.354	3.6767	3.517
0.737	3.316	3.6117	3.44
0.789	3.28	3.5423	3.358
0.842	3.244	3.466	3.269
0.895	3.21	3.384	3.174
0.947	3.177	3.298	3.075
1	3.145	3.2048	2.969

computational method. The results show that FPM aligns more closely with the Frozen Cargo data than HPM, demonstrating its ability to capture non-linear damping and restoring effects more effectively.

In Table 5, the comparison is restricted to HPM and FPM results under the same initial conditions. This comparison emphasizes the numerical reliability of the proposed FPM by showing that it produces results consistent with HPM while offering advantages such as fewer expansion terms reduced computational effort, and efficient handling of nonlinearities. While Table 4 establishes experimental validation, Table 5 provides numerical cross-validation, collectively showing that the FPM is both accurate and efficient. In order to forecast the time-series

Table 5. Numerical results of roll angle with HPM and FPM results.

t(Sec.)	HPM	FPM
0	9.8685	10
0.053	9.8683	9.9971
0.105	9.8632	9.9886
0.158	9.853	9.9743
0.211	9.8379	9.9541
0.263	9.8182	9.9287
0.316	9.7933	9.897
0.368	9.764	9.8603
0.421	9.7292	9.8172
0.474	9.6895	9.7683
0.526	9.6458	9.7147
0.579	9.5964	9.6543
0.632	9.5422	9.5881
0.684	9.4842	9.5175
0.737	9.4205	9.4398
0.789	9.3533	9.358
0.842	9.2801	9.2688
0.895	9.2022	9.1739
0.947	9.1213	9.0751
1	9.0342	8.9687

data, FPM results combined with MLP for various parameter values in the scaled data model. The performance of the ML-FPM has been validated against HPM and exact solution results.

The Fig. 4 presents a comparative study of roll angle decay over time using three approaches: Frozen Cargo, HPM, and FPM. The Frozen Cargo data, obtained from experimental or validated numerical studies, serves as the benchmark representing realistic roll behavior of a barge-like vessel. HPM consistently predicts higher roll angles, indicating slower decay and thus an underestimation of damping effects. In contrast, FPM closely matches the Frozen Cargo trend throughout most of the motion, with only a slight under prediction at later times,

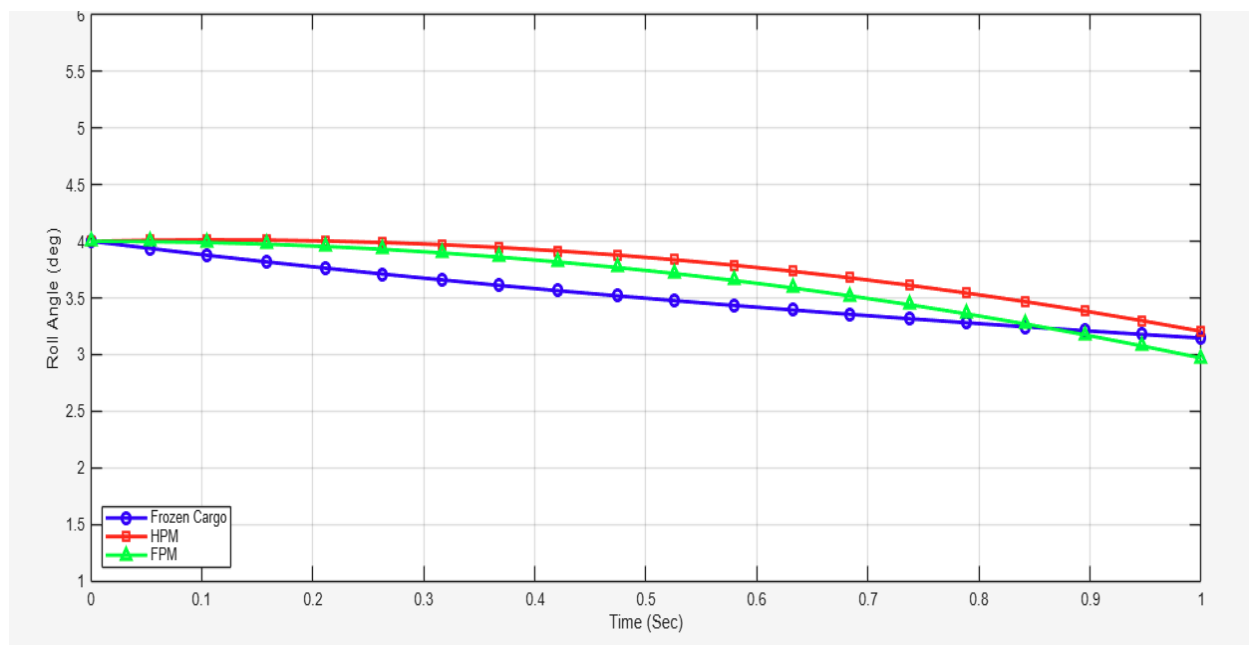


Fig. 4. Comparative analysis of FPM with experimental results and HPM at 4° roll angle.

reflecting a minor overestimation of damping. This demonstrates that FPM provides a more reliable representation of non-linear damping and restoring effects, making it a preferable computational approach for accurate roll dynamics analysis.

Figs. (5-7) shows the comparison of roll angle decay predicted by HPM and FPM over time. FPM closely follows the expected trend,

showing slightly faster decay than HPM, which tends to over predict roll angles. This highlights FPM's better accuracy in capturing damping effects. The proposed ML-FPM demonstrates superior alignment with Frozen Cargo and HPM for a range of time values. Specifically, ML-FPM outperforms traditional FPM by providing more consistent results across the entire interval. The efficiency of ML-FPM is further validated in

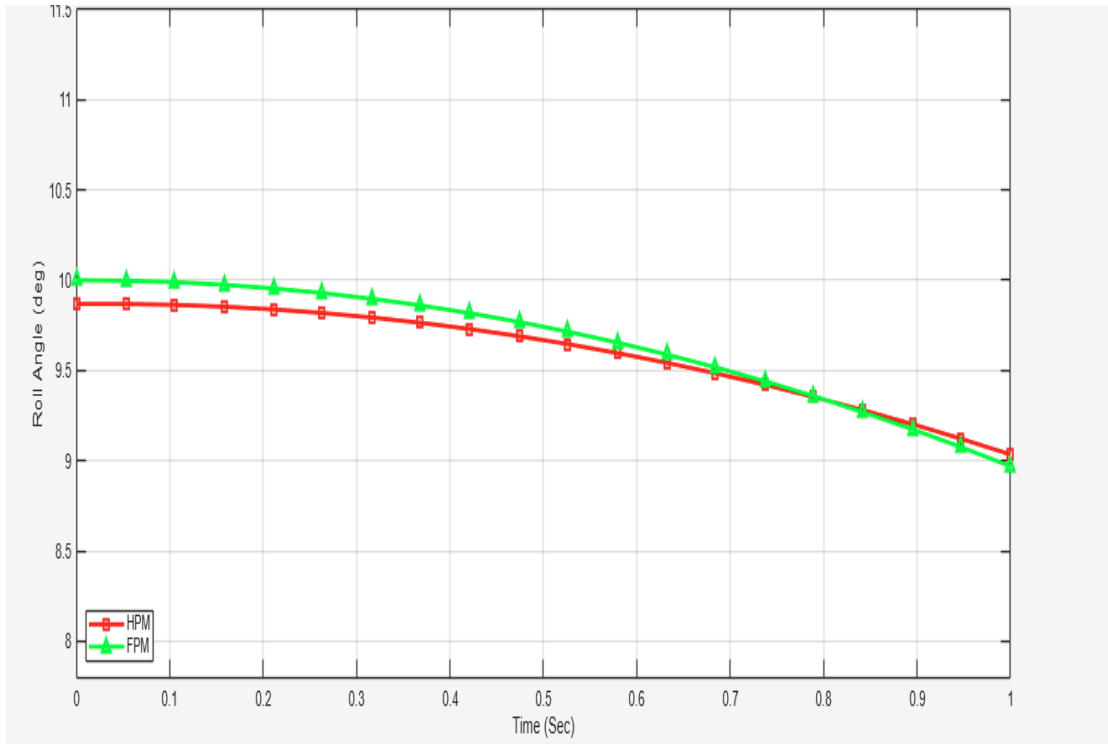


Fig. 5. Comparative analysis between FPM and HPM at 4° roll angle.

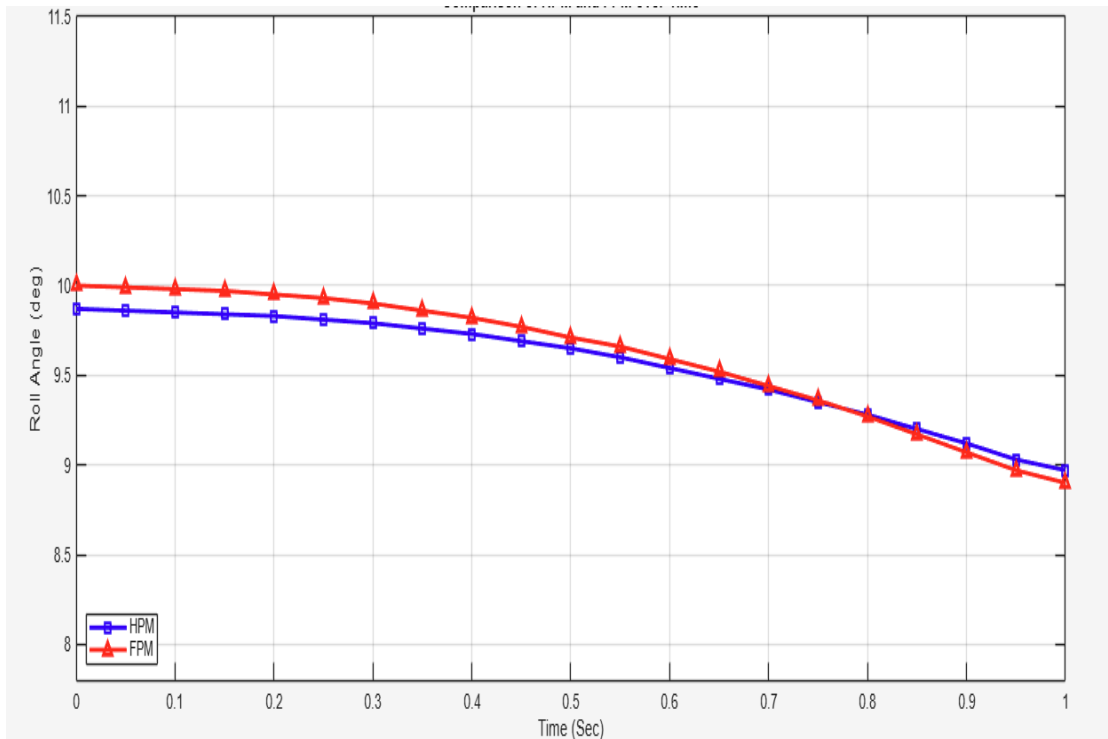


Fig. 6. Comparison between FPM and HPM for 4° roll angle.

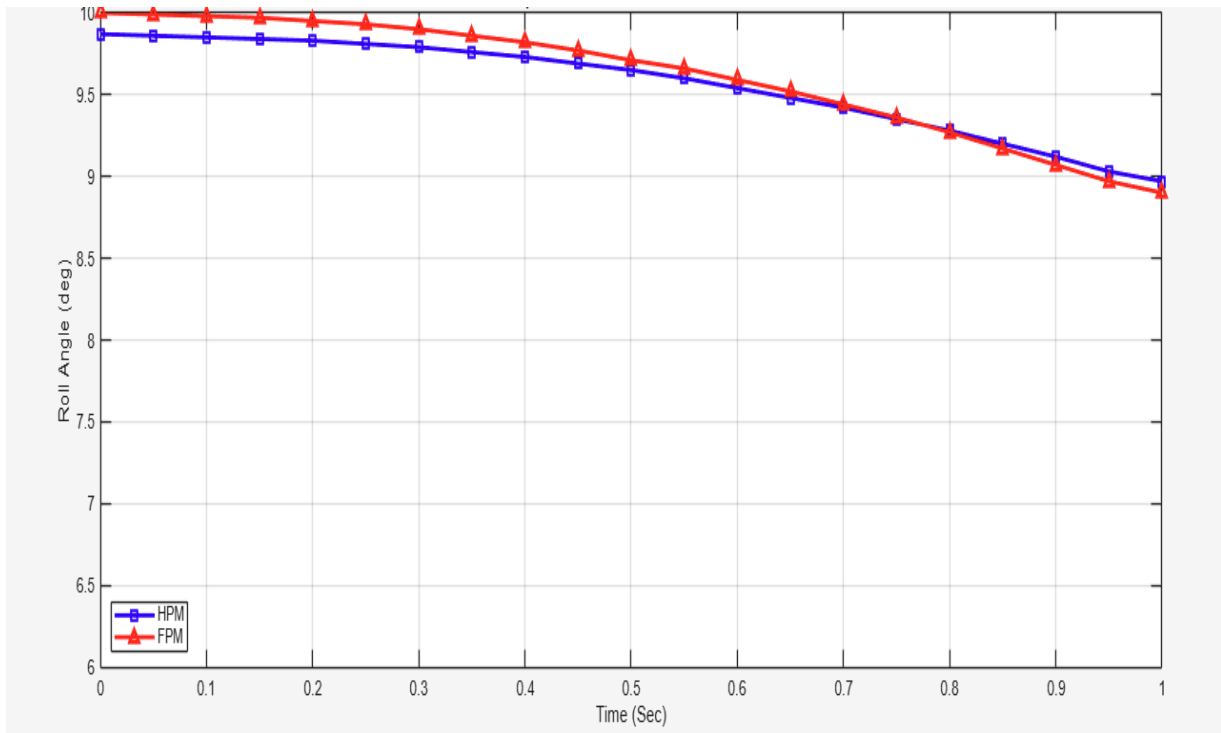


Fig. 7. Comparative study between FPM and HPM at 4° roll angle.

Figs. (8-11), which show that ML-FPM not only reduces computational complexity but also much coincidence with the experimental data sets. For instance, in Figure 8, ML-FPM closely matches HPM and experimental values even for longer time intervals, illustrating its stability and reliability.

Additionally, ML-FPM results exhibit faster convergence to experimental values, as highlighted in Figs. (12-15). Based on the observed regression performance across training, validation, and test datasets, the machine learning model demonstrates high predictive accuracy and strong generalization capability. The near-perfect

correlation in the training set confirms effective learning, while the consistent R values above 0.96 in validation and test sets indicate minimal over fitting and reliable extrapolation to unseen data. The alignment of regression slopes close to 1 and low intercepts across all datasets further supports the model’s calibration and bias-free behavior. In the context of ML-driven regression, such metrics reflect a well-tuned architecture with robust parameterization, making it suitable for deployment in physically grounded applications where precision and interpretability are critical. This indicates that Multi-layer Fermat polynomial method (ML-FPM), with its machine learning-enhanced framework, effectively

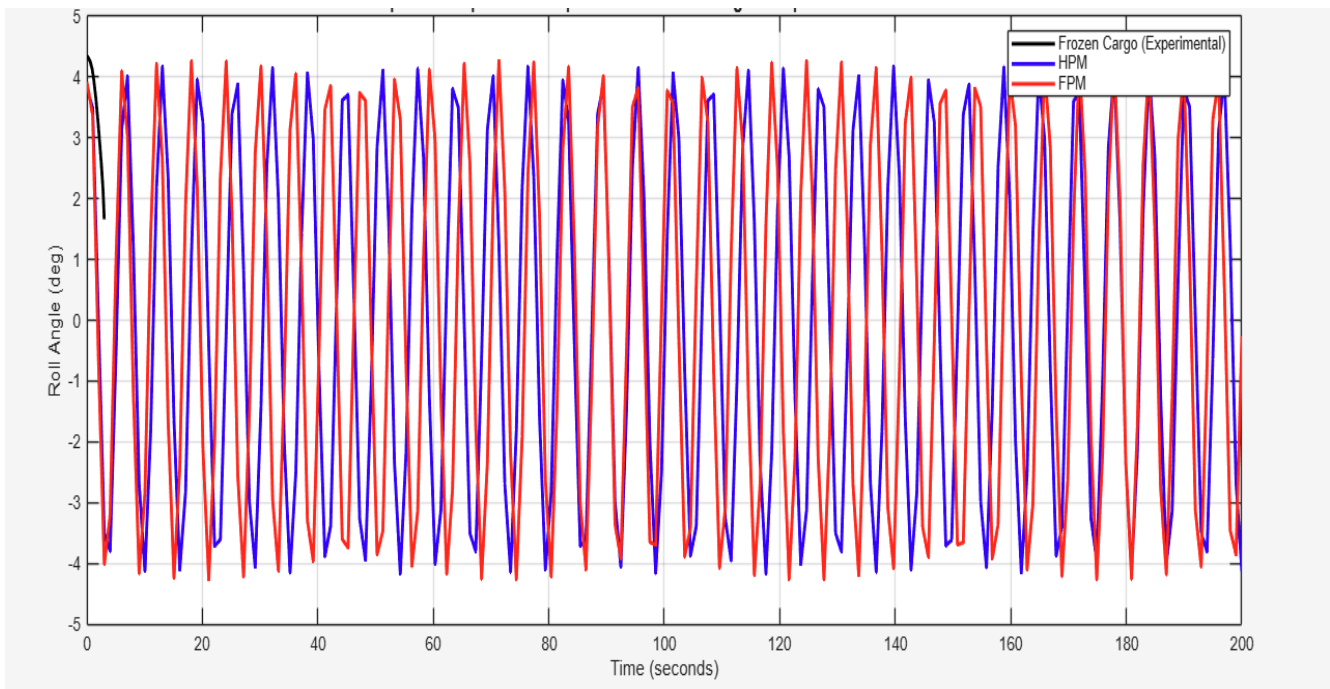


Fig. 8. Comparative analysis of ML-FPM, frozen cargo and HPM for 4° roll angle.

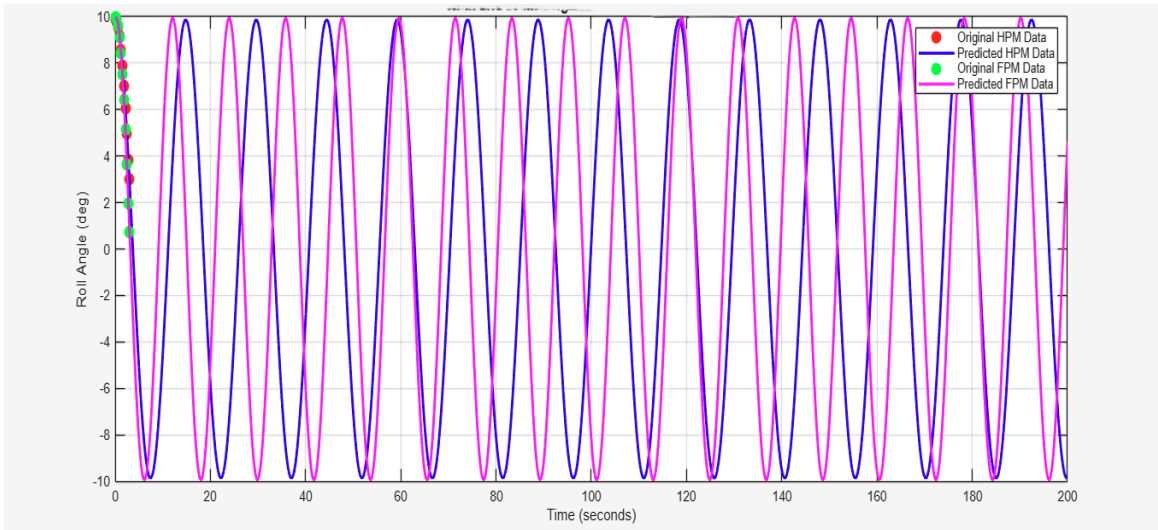


Fig. 9. Comparative analysis of ML-FPM and HPM for 10° roll angle.

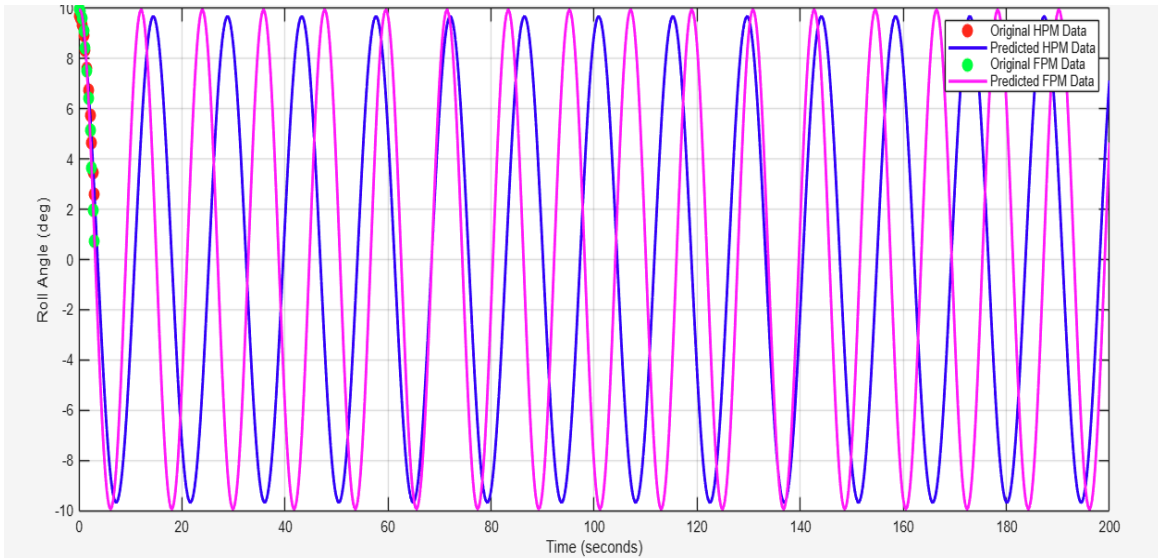


Fig. 10. Comparative study of ML-FPM and HPM at 10° roll angle.

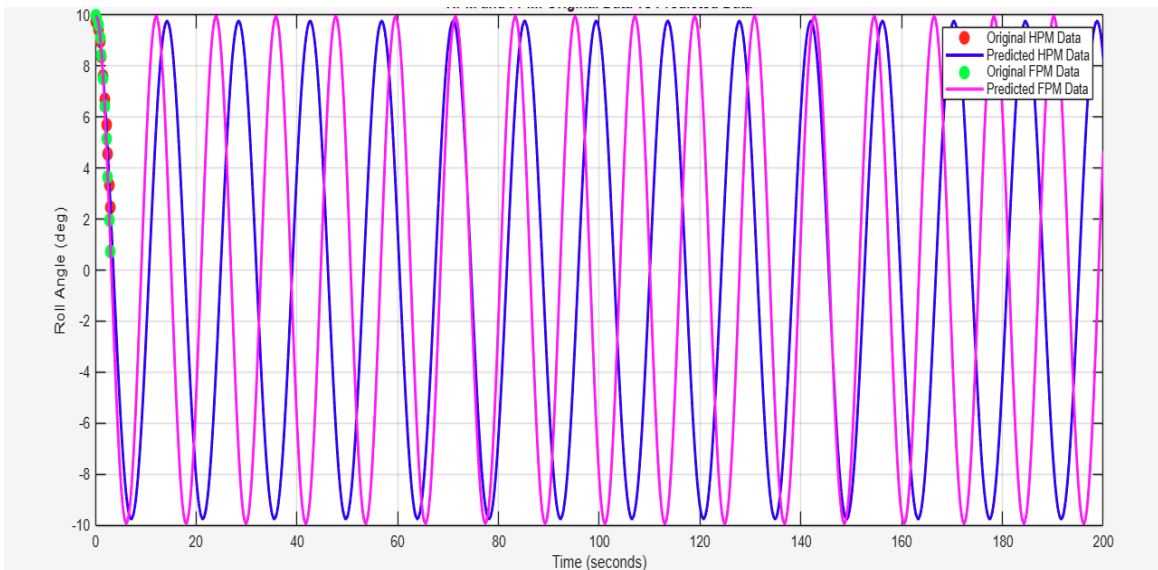


Fig. 11. Comparative analysis of ML-FPM and HPM at 10° roll angle.

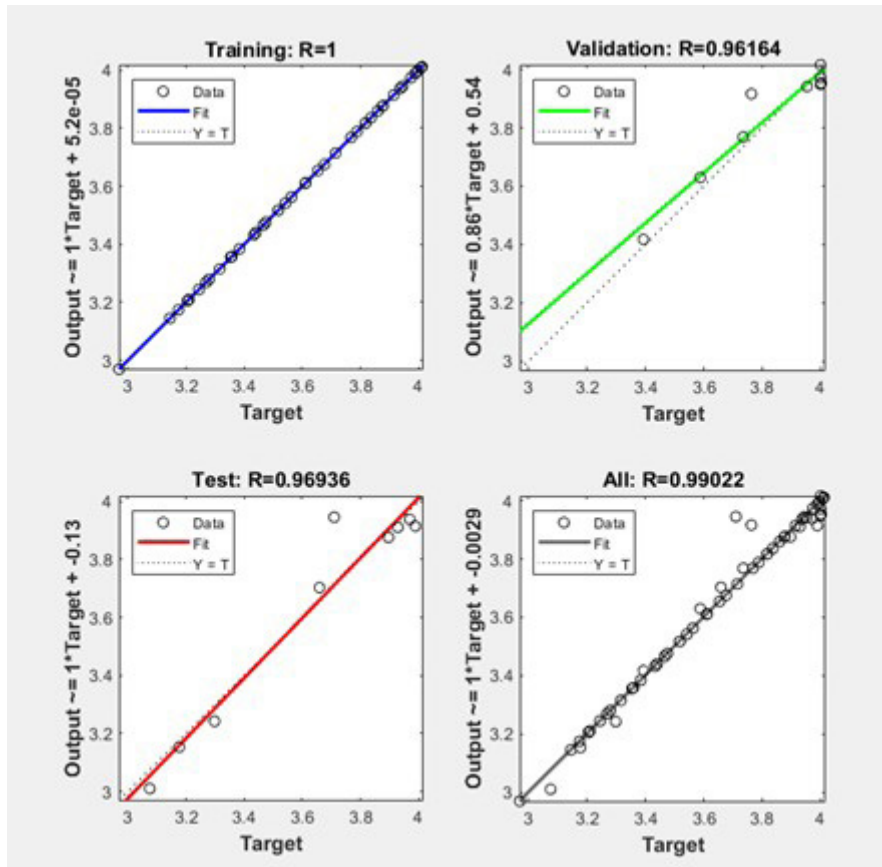


Fig. 12. R Estimate of ML-FPM (section 5.1).

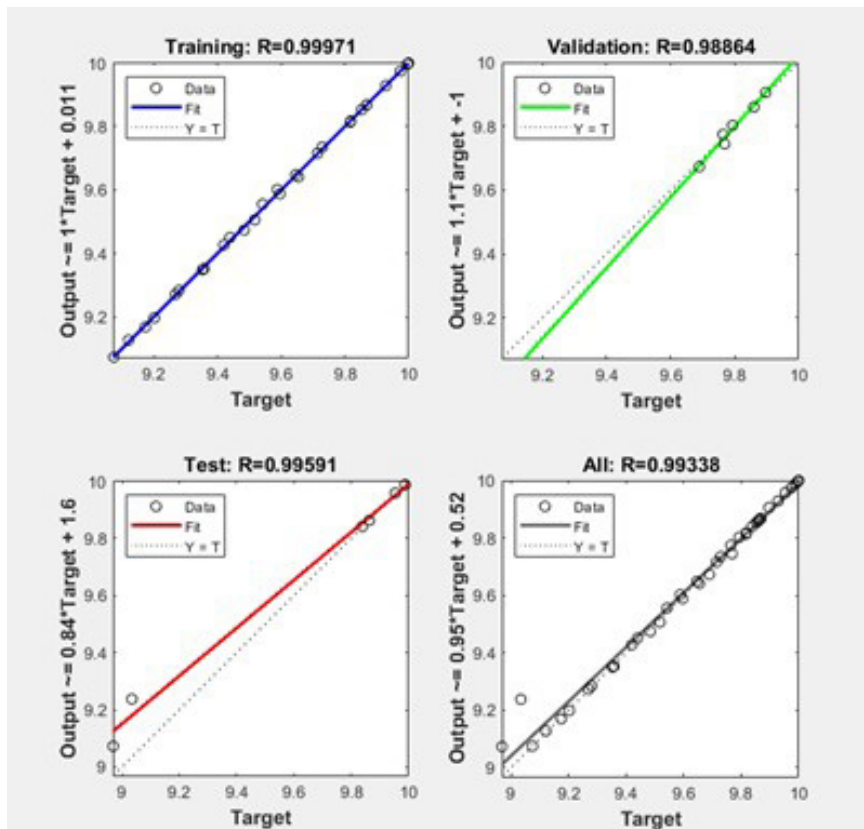


Fig. 13. R Estimate of ML-FPM (section 5.2-Case 1).

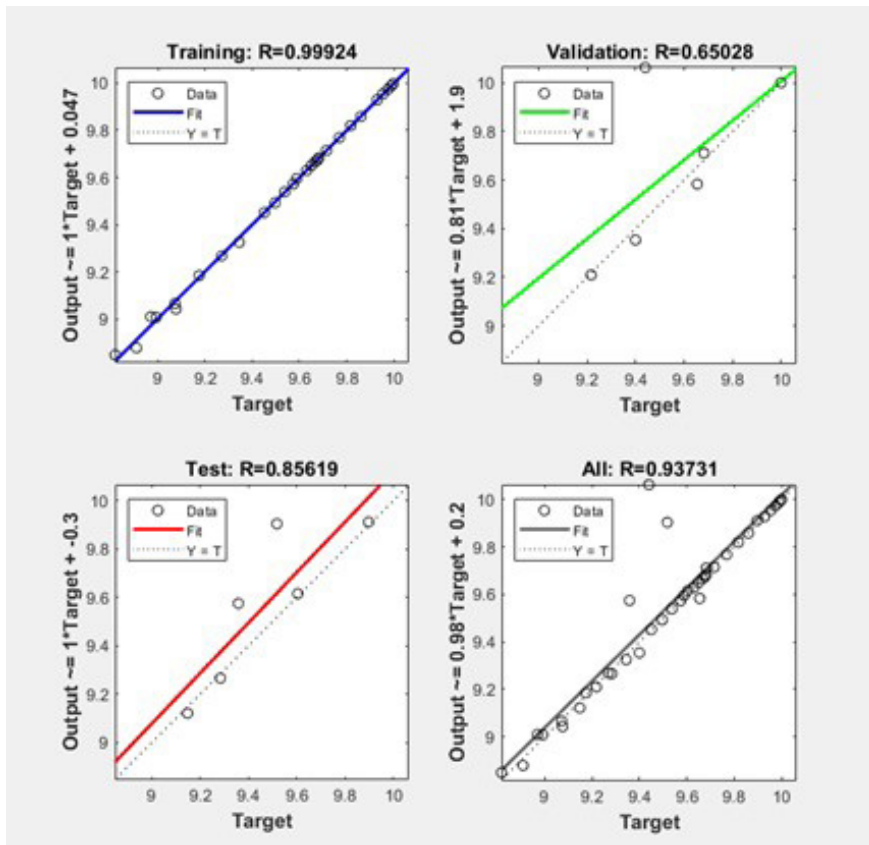


Fig. 14. R Estimate of ML-FPM (section 5.2-Case 2).

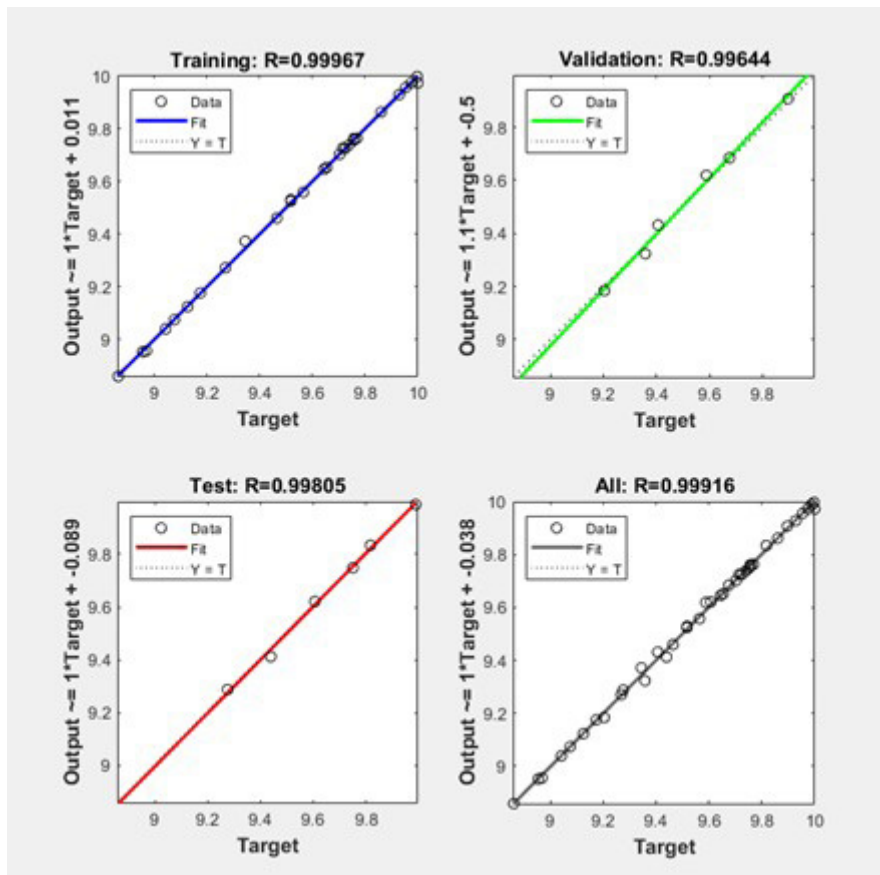


Fig. 15. R Estimate of ML-FPM (Section 5.2-Case 3).

compensates for non-linear behaviors and parameter variability. Hence, the numerical simulation and experimental validation assess the performance and efficiency of ML-FPM in terms of accuracy and computational cost. The proposed method achieves high precision with reduced computational effort, making it a viable alternative to existing techniques for ship roll angle prediction.

7. Future Work

In future we could explore extending the FPM framework to multi-degree-of-freedom ship motion models and irregular sea states. Incorporating adaptive learning strategies within the MLP architecture may enhance long-term roll angle forecasting. Additionally, hybridizing wavelet methods with data-driven techniques could improve robustness under varying damping and restoring conditions.

8. Conclusions

This research introduces a novel computational approach for predicting ship roll behavior by applying the ML-FPM to solve the system's non-linear dynamics. The accuracy and robustness of the technique have been assessed by comparison with both the HPM and empirical data from frozen cargo scenarios. The core aim is to establish and confirm a dependable predictive framework capable of estimating roll angles with high precision. In contrast to conventional techniques, the ML-FPM handles the original non-linear formulations directly, eliminating the need for simplifications or auxiliary transformation steps. The machine-learning enhancement significantly improves predictive accuracy by learning the non-linear dynamics and refining the solution space. Results indicate that the proposed ML-FPM method consistently achieves highly accurate approximate solutions with fewer terms in the approximate expansion, reducing computational complexity. For smaller time intervals, ML-FPM shows close agreement with HPM and frozen cargo results, while for larger time intervals, it maintains stability and precision. Comparative analysis against experimental and simulation data further validates its accuracy and applicability. The proposed ML-FPM is particularly efficient in handling the dynamics of roll motion with 1-Degree of Freedom (1-DOF). This is evident in its ability to produce solutions that closely match experimental results, even under varying non-linear conditions. The numerical experiments and graphical analyses clearly illustrate its superior performance in terms of convergence, accuracy, and reduced computational effort compared to traditional methods. In conclusion, the ML-FPM provides a robust and reliable computational framework for solving non-linear ship roll motion equations. Its ability to achieve accurate results with minimal computational overhead makes it a promising tool for extending to other ship motion models and real-time applications.

All simulations detailed in this section were carried out using Python scripts with double-precision arithmetic on a personal workstation. The computational environment consisted of a system labelled DESKTOP-QM2UOCJ, equipped with an 11th Generation Intel(R) Core(TM) i5-1135G7 processor running at 2.40 GHz (up to 2.42 GHz) and 8 GB of RAM.

CRedit authorship contribution statement

S. Krithikka: Writing original draft, writing, review & editing, methodology, investigation, formal analysis, conceptualization. **G. Hariharan:** Methodology, investigation, writing, review & editing, project administration, supervision, funding acquisition. **H. Jafari:** Investigation, review & editing, supervision.

Declaration of competing interest

The authors declare that they have no known competing financial interests or personal relationships that could have appeared to influence the work reported in this paper.

Data availability

Data sharing is not applicable to this article as no datasets were generated or analyzed during the current study.

Declaration of generative AI and AI-assisted technologies in the writing process

The authors confirm that there was no use of artificial intelligence (AI)-assisted technology for assisting in the writing or editing of the manuscript and no images were manipulated using AI.

Acknowledgments

The authors extend their heartfelt gratitude to the Editor and the anonymous reviewers for their invaluable feedback and constructive suggestions, which have significantly improved the quality and clarity of this paper. The authors gratefully acknowledge SASTRA Deemed University, Thanjavur, for the infrastructure support that facilitated this research. Financial assistance from SPARC-MHRD (Project Code: P3755), New Delhi, is also duly recognized and appreciated.

References

- Fernandes, A.C., Oliveira, A.C., 2009. The roll damping assessment via decay model testing (new ideas about an old subject). *J Marine Sci Appl* 8, 144-150. <https://doi.org/10.1007/s11804-009-8107-z>
- Hariharan, G., Kannan, K., 2014. Review of wavelet methods for the solution of reaction-diffusion problems in science and engineering. *Appl Math Model* 38, 799-813. <https://doi.org/10.1016/j.apm.2013.08.003>
- Hosseini, V., Remazani, M., Zou, W., Banihashemi, S., 2021. Stochastic model for multi-term time-fractional diffusion equations with noise. *Therm sci* 25, 287-293. <https://doi.org/10.2298/tsci21s2287h>
- Igbadumbe, J.F., Sallam, O., Fürth, M., Feng, R., 2020. Experimental determination of non-linear roll damping of an FPSO pure roll coupled with liquid sloshing in two-row tanks. *JMSE* 8, 582. <https://doi.org/10.3390/jmse8080582>
- Irkal, M.A.R., Nallayarasu, S., Bhattacharyya, S.K., 2016. CFD approach to roll damping of ship with bilge keel with experimental validation. *Appl Ocean Res* 55, 1-17. <https://doi.org/10.1016/j.apor.2015.11.008>
- Jafari, H., Malidareh, B.F., Hosseini, V.R., 2024. Collocation discrete least squares meshless method for solving non-linear multi-term time fractional differential equations. *Eng Anal Bound Elem* 158, 107-120. <https://doi.org/10.1016/j.enganabound.2023.10.014>
- Kim, Y., Park, M.J., 2015. Identification of the non-linear roll damping and restoring moment of a FPSO using Hilbert transform. *Ocean Eng* 109, 381-388. <https://doi.org/10.1016/j.oceaneng.2015.09.019>
- Nduka, M.U., Oruh, B.I., 2022. A Fermat polynomial method for solving optimal control problems. *International Journal of Mathematical Analysis and Modelling* 5, 56-68.
- Rodriguez, C.A., Ramos, I.S., Esperança, P.T.T., Oliveira, M.C., 2020. Realistic estimation of roll damping coefficients in waves based on model tests and numerical simulations. *Ocean Eng* 213, 107664. <https://doi.org/10.1016/j.oceaneng.2020.107664>
- ShadabFar, M., Mahsuli, M., Khojine, A.S., Hosseini, V.R., Hong, A., 2023. Randomized fractional SEIR-VQHP model with applications in covid-19 data prediction. *Fractals* 31. <https://doi.org/10.1142/s0218348x23400649>
- Swaminathan, G., G, H., Ganeshan, S., Ayyangar, V.B.S., 2022. A wavelet approximation method for solving non-linear ship roll damping equations: An operational matrix of derivative approach. *Ocean Eng* 264, 112390. <https://doi.org/10.1016/j.oceaneng.2022.112390>
- Yousri, Y.H., 2017. A new operational matrix of Caputo fractional derivatives of Fermat polynomials: An application for solving the Bagley-Torvik equation. *Adv Differ Equ* 2017. <https://doi.org/10.1186/s13662-017-1123-4>
- Zhao, W., McPhail, F., 2017. Roll response of an LNG carrier considering the liquid cargo flow. *Ocean Eng* 129, 83-91. <https://doi.org/10.1016/j.oceaneng.2016.11.023>
- Zhao, W., Efthymiou, M., McPhail, F., Wille, S., 2016. Non-linear roll damping of a barge with and without liquid cargo in spherical tanks. *J Ocean Eng Sci* 1, 84-91. <https://doi.org/10.1016/j.joes.2015.12.002>
- Zhao, W., McPhail, F., Efthymiou, M., 2016. Effect of partially filled spherical cargo tanks on the roll response of a barge-like vessel. *J Offshore Mech Arctic Eng* 138. <https://doi.org/10.1115/1.4032658>